Enhancement of self-collimated fields in photonic crystals consisting of two kinds of single-negative materials

Zi-li Wang,[1,2] Hai-tao Jiang,[1,2,*] Yun-hui Li,[1,2] and Hong Chen[1,2]

[1] *Pohl Institute of Solid State Physics, Tongji University, Shanghai, 200092, China*
[2] *Shanghai Key Laboratory of Special Artificial Microstructure Materials and Technology, Shanghai, 200092, China*
**jiang-haitao@tongji.edu.cn*

Abstract: Self-collimations are found in one-dimensional (1D) photonic crystals consisting of two kinds of single-negative materials that effectively cancel each other out. Compared to the self-collimations in all-dielectric photonic crystals or 1D photonic crystals with negative-index materials, this kind of structure can amplify both far and near fields greatly during collimation.

OCIS codes: (160.5298) photonic crystals; (160.3918) metamaterials; (120.1680) Collimation.

References and links

1. H. Kosaka, T. Kawashima, A. Tomita, M. Notomi, T. Tamamura, T. Sato, and S. Kawakami, "Self-collimating phenomena in photonic crystals," Appl. Phys. Lett. **74**(9), 1212 (1999).
2. D. N. Chigrin, S. Enoch, C. Sotomayor Torres, and G. Tayeb, "Self-guiding in two-dimensional photonic crystals," Opt. Express **11**(10), 1203–1211 (2003).
3. C. Y. Luo, S. G. Johnson, J. D. Joannopoulos, and J. B. Pendry, "Subwavelength imaging in photonic crystals," Phys. Rev. B **68**(4), 045115 (2003).
4. Z. Y. Li, and L. L. Lin, "Evaluation of lensing in photonic crystal slabs exhibiting negative refraction," Phys. Rev. B **68**(24), 245110 (2003).
5. P. A. Belov, C. R. Simovski, and P. Ikonen, "Canalization of subwavelength images by electromagnetic crystals," Phys. Rev. B **71**(19), 193105 (2005).
6. P. T. Rakich, M. S. Dahlem, S. Tandon, M. Ibanescu, M. Soljacić, G. S. Petrich, J. D. Joannopoulos, L. A. Kolodziejski, and E. P. Ippen, "Achieving centimetre-scale supercollimation in a large-area two-dimensional photonic crystal," Nat. Mater. **5**(2), 93–96 (2006).
7. R. E. Hamam, M. Ibanescu, S. G. Johnson, J. D. Joannopoulos, and M. Soljacić, "Broadband super-collimation in a hybrid photonic crystal structure," Opt. Express **17**(10), 8109–8118 (2009).
8. Z. L. Lu, S. Y. Shi, J. A. Murakowski, G. J. Schneider, C. A. Schuetz, and D. W. Prather, "Experimental demonstration of self-collimation inside a three-dimensional photonic crystal," Phys. Rev. Lett. **96**(17), 173902 (2006).
9. X. F. Yu, and S. H. Fan, "Bends and splitters for self-collimated beams in photonic crystals," Appl. Phys. Lett. **83**(16), 3251 (2003).
10. M.-W. Kim, S.-G. Lee, T.-T. Kim, J.-E. Kim, H. Y. Park, and C.-S. Kee, "Experimental demonstration of bending and splitting of self-collimated beams in two-dimensional photonic crystals," Appl. Phys. Lett. **90**(11), 113121 (2007).
11. B. L. Miao, C. H. Chen, S. Y. Shi, and D. W. Prather, "A high-efficiency in-plane splitting coupler for planar photonic crystal self-collimation devices," IEEE Photon. Technol. Lett. **17**(1), 61–63 (2005).
12. D. Y. Zhao, J. Zhang, P. J. Yao, X. Y. Jiang, and X. Y. Chen, "Photonic crystal Mach-Zehnder interferometer based on self-collimation," Appl. Phys. Lett. **90**(23), 231114 (2007).
13. J. B. Pendry, "Negative refraction makes a perfect lens," Phys. Rev. Lett. **85**(18), 3966–3969 (2000).
14. R. A. Shelby, D. R. Smith, and S. Schultz, "Experimental verification of a negative index of refraction," Science **292**(5514), 77–79 (2001).
15. J. B. Pendry, A. J. Holden, W. J. Stewart, and I. Youngs I, "Extremely low frequency plasmons in metallic mesostructures," Phys. Rev. Lett. **76**(25), 4773–4776 (1996).
16. J. B. Pendry, A. J. Holden, D. J. Robbins, and W. J. Stewart, "Magnetism from conductors and enhanced nonlinear phenomena," IEEE Trans. Microw. Theory Tech. **47**(11), 2075–2084 (1999).
17. A. N. Grigorenko, A. K. Geim, H. F. Gleeson, Y. Zhang, A. A. Firsov, I. Y. Khrushchev, and J. Petrovic, "Nanofabricated media with negative permeability at visible frequencies," Nature **438**(7066), 335–338 (2005).
18. V. Mocella, S. Cabrini, A. S. Chang, P. Dardano, L. Moretti, I. Rendina, D. Olynick, B. Harteneck, and S. Dhuey, "Self-collimation of light over millimeter-scale distance in a quasi-zero-average-index metamaterial," Phys. Rev. Lett. **102**(13), 133902 (2009).

#126182 - $15.00 USD Received 30 Mar 2010; revised 10 Jun 2010; accepted 16 Jun 2010; published 21 Jun 2010

19. K. J. Webb, and M. C. Yang, "Generation and control of optical vortices using left-handed materials," Phys. Rev. E Stat. Nonlin. Soft Matter Phys. **74**(1), 016601 (2006).
20. J. Li, L. Zhou, C. T. Chan, and P. Sheng, "Photonic band gap from a stack of positive and negative index materials," Phys. Rev. Lett. **90**(8), 083901 (2003).
21. H. T. Jiang, H. Chen, H. Q. Li, Y. W. Zhang, J. Zi, and S. Y. Zhu, "Properties of one-dimensional photonic crystals containing single-negative materials," Phys. Rev. E Stat. Nonlin. Soft Matter Phys. **69**(6), 066607 (2004).
22. A. Alu, and N. Engheta, "Pairing an epsilon-negative slab with a mu-negative slab: resonance, tunneling and transparency," IEEE Trans. Antenn. Propag. **51**(10), 2558–2571 (2003).
23. C. M. Rappaport, and B. J. McCartin, "FDFD analysis of electromagnetic scattering in anisotropic media using unconstrained triangular meshes," IEEE Trans. Antenn. Propag. **39**(3), 345–349 (1991).
24. J. L. Zhang, H. T. Jiang, W. D. Shen, X. Liu, Y. Y. Li, and P. F. Gu, "Omnidirectional transmission bands of one-dimensional metal-dielectric periodic structures," J. Opt. Soc. Am. B **25**(9), 1474 (2008).
25. S. Zouhdi, A. V. Dorofeenko, A. M. Merzlikin, and A. P. Vinogradov, "Theory of zero-width band gap effect in photonic crystals made of metamaterials," Phys. Rev. B **75**(3), 035125 (2007).
26. J. A. Kong, B. L. Wu, and Y. Zhang, "Lateral displacement of a Gaussian beam reflected from a grounded slab with negative permittivity and permeability," Appl. Phys. Lett. **80**(12), 2084 (2002).
27. J. Zhang, H. Jiang, B. Gralak, S. Enoch, G. Tayeb, and M. Lequime, "Compensation of loss to approach −1 effective index by gain in metal-dielectric stacks," Eur. Phys. J. Appl. Phys. **46**(3), 32603 (2009).
28. Y. Sivan, S. M. Xiao, U. K. Chettiar, A. V. Kildishev, and V. M. Shalaev, "Frequency-domain simulations of a negative-index material with embedded gain," Opt. Express **17**(26), 24060–24074 (2009).
29. Z. G. Dong, H. Liu, T. Li, Z. H. Zhu, S. M. Wang, J. X. Cao, S. N. Zhu, and X. Zhang, "Optical loss compensation in a bulk left-handed metamaterial by the gain in quantum dots," Appl. Phys. Lett. **96**(4), 044104 (2010).

1. Introduction

In the control of electromagnetic fields, self-collimation that can overcome beam spreading caused by diffraction is an important phenomenon. Self-collimation in 2D or 3D dielectric photonic crystals (PCs) has been discovered and used to bend and split light beam in integrated photonic circuits and design a Mach-Zehnder interferometer [1–12]. In general, the collimated fields in the dielectric PCs are not strong since the waves are traveling Bloch waves. Recently, much attention has been attracted to metamaterials that mainly include double-negative (DNG) materials ($\varepsilon < 0, \mu < 0$) [13,14] and single-negative materials including epsilon-negative (ENG) materials ($\varepsilon < 0, \mu > 0$) [15] and mu-negative (MNG) materials ($\varepsilon > 0, \mu < 0$) [16,17]. In 2009, V. Mocella et al. found that a 1D PC composed of an effective DNG material with index of −1 and air (for simplicity, this structure is called 'DNG/air PC') could also collimate light beam because of the negative refraction across every interface between the two media that optically cancel each other out [18]. When the incident beam contains evanescent wave component, optical vortices [18,19] that occur in the structure can facilitate the transportation of evanescent waves. So this structure can collimate near fields.

In this paper, we find that self-collimation can also appear in a 1D PC consisting of MNG and ENG media (for simplicity, this structure is called 'MNG/ENG PC'). The physical mechanism of this self-collimation will be explained in details in the next section. Similar to DNG/air PC, MNG/ENG PC can also collimate near fields. However, the transportation mechanisms of far fields (propagating wave component) in two kinds of PCs are quite different. In a DNG/air PC, an incident propagating wave is transported in the form of a traveling wave due to the interference of forward and backward propagating waves in air and DNG material [20]. But in MNG or ENG media, in the propagation direction, the wave should be evanescent wave since the wavevector is complex. So in MNG/ENG PCs the transportation of an incident propagating wave is based on the tunneling mechanism of evanescent waves in MNG and ENG media. Compared to DNG/air PC, both far and near fields can be collimated and greatly amplified in MNG/ENG PC. The enhancement of fields can decrease the velocity of light and boost the nonlinear effect noticeably. This self-collimated slow wave is highly desirable in some applications.

#126182 - $15.00 USD Received 30 Mar 2010; revised 10 Jun 2010; accepted 16 Jun 2010; published 21 Jun 2010

2. Mechanism of self-collimation in MNG/ENG PC

Figure 1(a) is a schematic of a MNG/ENG PC with three periods that is surrounded by air. The thickness of a MNG layer that is denoted by d_1 is the same with that of an ENG layer denoted by d_2. The permeability and permittivity of MNG and ENG media are supposed to be

$$\mu_1=\mu_a-\frac{\alpha^2}{(2\pi f)^2},\quad \varepsilon_1=\varepsilon_a, \tag{1}$$

and

$$\mu_2=\mu_b,\quad \varepsilon_2=\varepsilon_b-\frac{\beta^2}{(2\pi f)^2}, \tag{2}$$

respectively, where f is frequency. At visible frequencies, typical metals are ENG media below the plasma frequency. Recently, low-loss MNG media have also been fabricated at near-visible frequencies [17]. In the following calculations, we choose $\alpha=\beta=2\pi\times10^3$ in units of terahertz (THz), $\mu_a=3,\varepsilon_a=1,\mu_b=1,\varepsilon_b=3$. At these parameters, we can obtain $\mu_1=-1,\varepsilon_1=1,\mu_2=1,\varepsilon_2=-1$ (conjugated match parameters [22]) when f=500 THz.

It is known that a monochromatic Gaussian beam contains both propagating wave and evanescent wave components. When the width of a Gaussian beam is larger than or in the scale of the incident wavelength, the beam mainly contains propagating wave components. But when the width of a Gaussian beam is much smaller than the incident wavelength, the beam mainly contains evanescent wave components. Here, we study the first case. In Fig. 1(a), a plane wave at frequency of 500 THz impinges on the PC in which the lattice constant is 312 nm at an angle of 30 degree. The plane wave is a transverse electric (TE) wave, i.e., the electric field is in y direction. We suppose the square of electric fields ($|E_y|^2$) of incident wave is 1. Then we use Finite Difference Frequency Domain (FDFD) method [23] to simulate the energy flow and $|E_y|^2$ in the PC. Square meshes and perfectly matched layer (PML) boundaries are used. The size of computational grid is 2 nm. In Fig. 1(a) it is seen that the component of energy flow parallel to interface (S_x) reverses when light runs across the interface because of the continuous conditions of boundary [24]. When the two types of media effectively cancel each other out ($\varepsilon_1 d_1+\varepsilon_2 d_2=0,\mu_1 d_1+\mu_2 d_2=0$), S_x in two media can totally compensate each other. In this case, over the entire length of PC, the energy flow can be seen as only propagating in z direction. Moreover, in Fig. 1(a) the energy flow in MNG or ENG medium gradually changes its direction and the value of $|E_y|^2$ increases to 16 at every MNG/ENG interface. For comparison, in Fig. 1(b) we also calculate the distributions of energy flow and $|E_y|^2$ when the same plane wave impinges on a DNG/air PC. In contrast to Fig. 1(a), the energy flow maintains its direction in a single layer and $|E_y|^2$ is 1 everywhere. The different field patterns in Figs. 1(a) and 1(b) are due to the different transportation mechanisms of incident propagating wave in two kinds of PCs. In Fig. 1(c) we numerically show the distributions of energy flow and $|E_y|^2$ in MNG/ENG PC impinged by a Gaussian beam. The distribution of the Gaussian beam in the total field-scattered field plane is $\exp(-x^2/g^2)$, where the width $2g$ = 660 nm. The distance between beam source and the front of the first MNG layer is 100 nm. It is seen that the energy flows at the exit face of the

#126182 - $15.00 USD Received 30 Mar 2010; revised 10 Jun 2010; accepted 16 Jun 2010; published 21 Jun 2010

PC are the same with those at the entrance face. Inside PC, the beam is refocused at every MNG/ENG interface and the size of beam spot is unchanged, leading to a self-collimation over the entire length of PC. Since the conjugated match parameters are independent of incident angle and polarizations, the compensation effect of parallel component of energy flow can occur at any angle of incidence. So a Gaussian beam containing plane wave components in all directions can self-collimate in MNG/ENG PC.

Here we further confirm the self-collimation by calculating the equi-frequency contour (EFC) of the MNG/ENG PC. Based on the Bloch-Floquet theorem, the dispersion relation of the PC for a TE wave can be written as

$$\cos(K_z d) = \cos(\gamma_1 d_1)\cos(\gamma_2 d_2) - \frac{\gamma_1^2 \mu_2^2 + \gamma_2^2 \mu_1^2}{2\gamma_1 \gamma_2 \mu_1 \mu_2} \sin(\gamma_1 d_1)\sin(\gamma_2 d_2), \qquad (3)$$

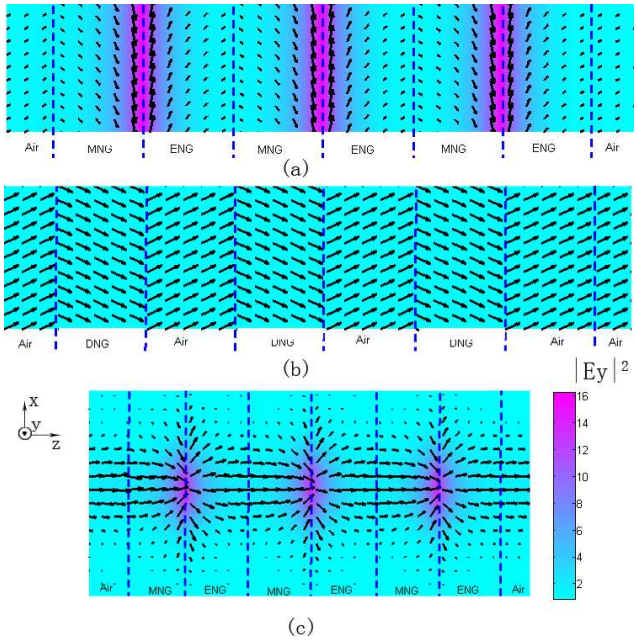

Fig. 1. Profile of the real part of the Poynting vector and $|E_y|^2$ in a (a) MNG/ENG PC at conjugated parameters and (b) a DNG ($\varepsilon = \mu = -1$) /air PC for a TE plane wave of 500 THz at an incident angle of 30 degree. (c) Profile of Poynting vector and $|E_y|^2$ in the same structure used in (a) for a Gaussian beam whose width is 660 nm. The distance between beam source and structure is 100 nm. The lattice constant in each PC is 312 nm and the thicknesses of the two media in a period are identical.

where *x*, *y* and *z* coordinates are indicated in Fig. 1, K_z is Bloch wave vector, $d = d_1 + d_2$, $\gamma_i = \sqrt{k_0^2 \varepsilon_i \mu_i - k_x^2}$ (i = 1, 2 denotes MNG and ENG media, respectively) and $k_0 = \omega / c$ is the wave number in the air. According to $\vec{\upsilon}_g = \vec{\nabla}_{\vec{k}} \omega(\vec{k})$, the direction of propagation (in the real space) is perpendicular to the EFC (in k-space). Figure 2 is calculated using $d_1 = d_2 = 50$ nm. In Fig. 2, the EFC at 500 THz is completely flat along *x* direction. It means that at 500 THz if the light is incident from the air at all angles of incidence ($-1 \le k_x / k_0 \le 1$), the light in the PC will perfectly collimate in z direction. Away from 500 THz, the EFCs will gradually deviate from flatness and those below 500 THz change much more slowly than those above 500 THz. To study the effect of collimation when the frequency deviates from 500 THz, we

#126182 - $15.00 USD Received 30 Mar 2010; revised 10 Jun 2010; accepted 16 Jun 2010; published 21 Jun 2010

simulate the distributions of the square of electric fields from 500 to 430 THz. The width of incident Gaussian beam is 1200 nm. We find even at 430 THz, after propagating for a distance of 5360 nm, the width of the beam only extends to 1260 nm. So, in a relatively broadband frequency range of 430 to 500 THz, the beam can be well collimated.

In Sections 3 and 4, the propagation of near fields or/and far fields in MNG/ENG PCs are studied.

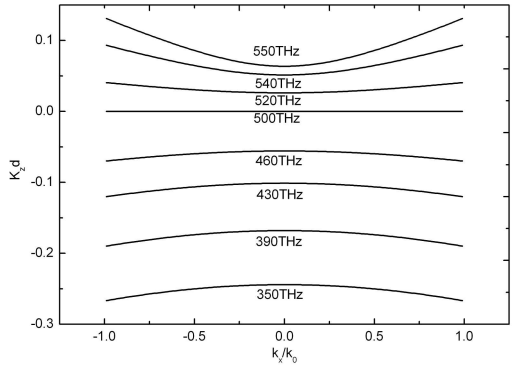

Fig. 2. The EFCs of a MNG/ENG PC in which $d_1 = d_2 = 50$ nm when the frequency varies from 350 to 550 THz. The EFC at 500 THz is completely flat. Away from 500 THz, the EFCs will gradually deviate from flatness and those below 500 THz change much more slowly than those above 500 THz.

3. Subwavelength collimation

In normal materials, a light source whose size is smaller than half wavelength cannot be imaged due to the absence of evanescent waves in the propagation. However, Pendry discovered negative refraction can overcome the diffraction limitation [13]. Later, S. Zouhdi et al. found that at conjugated match parameters MNG/ENG PCs can transport waves with any value of tangential component of wave number (k_x) [25], even when $k_x > k_0$ that corresponds to evanescent waves. Here we further confirm that subwavelength collimation can be realized in MNG/ENG PCs by using FDFD method. In simulation, square meshes and PML boundaries are used and the size of computational grid is 0.2 nm. In Fig. 3(a), a Gaussian beam source in air is 40 nm away from a metal plate with two very narrow slits. The incident wavelength and the width of the Gaussian beam are 600 nm and 360 nm, respectively. The width of slit is 60 nm. The distance between the centers of the two slits is 180 nm and the distance between the metal and MNG/ENG PC in which $d_1 = d_2 = 12$ nm is 2nm. When the Gaussian

#126182 - $15.00 USD Received 30 Mar 2010; revised 10 Jun 2010; accepted 16 Jun 2010; published 21 Jun 2010

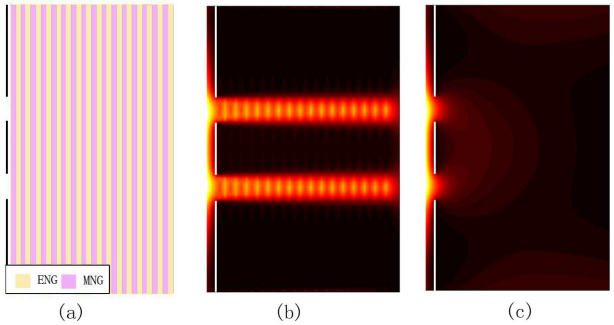

Fig. 3. (a) A structure with two slits in which $d_1 = d_2 = 12$ nm and the width of slit is 60 nm that is one tenth of the incident wavelength. Black strips denote metals. The distance between the centers of the two slits is 180 nm and the distance between the metal and MNG/ENG PC is 2 nm. The Gaussian beam source with 2g = 360 nm is 40 nm away from the metal plate. The distributions of square of electrical field show that two narrow beams are well separated and collimated in the structure (b) while extended and mixed in air (c).

beam transmits through two narrow slits, two beams with width much smaller than one wavelength are generated. In Fig. 3(b), it is seen that these two beams are well separated and collimated while propagating in the PC. Conversely, these two beams will strongly extended and mixed if they propagate in the air as shown in Fig. 3(c).

4. Enhancement of self-collimated fields

Since the matching frequency is invariant with the scaling change of the lattice constant [21], we can modify the field pattern of collimated beam by adjusting the lattice constant without changing the frequency of the beam. To demonstrate this point, we use a 2D transmission-matrix method [26] to simulate self-collimation propagations in two MNG/ENG PCs with different lattice constants. In this method, the incident Gaussian beam can be written as:

$$E_y = \int_{-\infty}^{\infty} \exp i(k_x x + k_{0z} z)\psi(k_x)dk_x, \tag{4}$$

where

$$\psi(k_x) = \frac{g}{2\sqrt{\pi}} \exp\{-[g^2 k_x^{\,2}/4]\}, \tag{5}$$

In Eqs. (4) and (5), g is half width of a Gaussian beam. The working wavelength is 600 nm and the length of each PC is 5360 nm. We suppose the intensity of the center of the incident beam is 1. The distance between beam source and structure is 120 nm. Firstly we choose g = 600 nm. In this case, the Gaussian beam mainly contains propagating wave components. As seen in Fig. 4(a), when lattice constant is 536 nm, a set of peaks of square of electric field occurs at every MNG/ENG interface and the field is highly localized around these interfaces. Though the absolute product of ε and μ is only 1 in MNG or ENG medium, the peak value of enhanced field is more than **140** times of incident field. From the top view shown by the inset, one can see the width of the field in *x* direction keeps unchanged. It means the field is confined in both lateral and longitudinal directions. The strong localization of fields can lead to a great reduction in group velocity and a significant enhancement of nonlinear interactions. As the lattice constant decreases, the localized strength at every MNG/ENG interface will decrease and this coupled localized field will gradually become a traveling wave. As shown in Fig. 4(b), when lattice constant is shortened to 67 nm, the collimated field is almost the same with incident field. Therefore, in MNG/ENG PC the pattern of collimated fields can be tuned either like a coupled localized field or a traveling wave. For comparison, in Figs. 4(c) and 4(d) we also calculate the distributions of square of the field in DNG/air PCs. All the other

#126182 - $15.00 USD Received 30 Mar 2010; revised 10 Jun 2010; accepted 16 Jun 2010; published 21 Jun 2010

parameters are the same with those in Figs. 4(a) and 4(b), respectively. From Figs. 4(c) and 4(d) we can see DNG/air PC always supports traveling waves no matter how the lattice constant varies. So for a wide Gaussian beam source, a MNG/ENG PC has more freedom to tune the collimated field. In details, if we want a collimated traveling wave, we only need to decrease the lattice constant. However, if we need strong localization

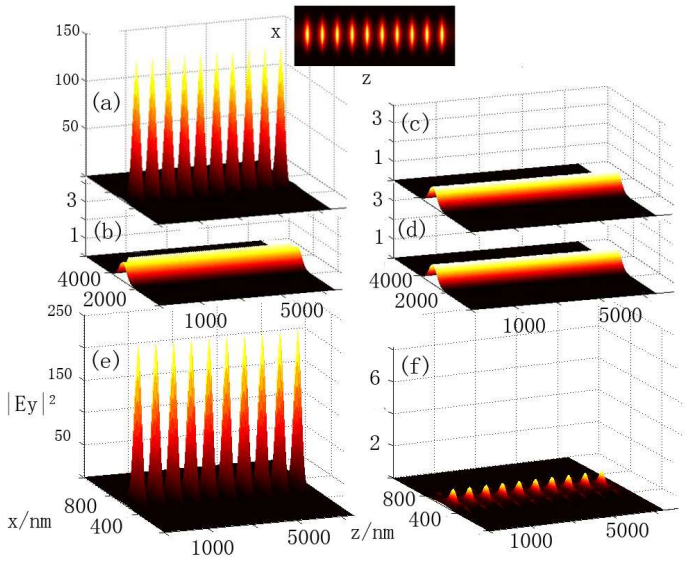

Fig. 4. Distributions of square of electrical fields in different PCs impinged by a Gaussian beam. g = 600 nm in (a)-(d) and g = 120 nm in (e) and (f), respectively. Total length of each PC is 5360 nm. Left column with (a), (b) and (e): MNG/ENG PCs. (a) lattice constant is 536 nm. g = 600 nm. The inset is the top view. (b) lattice constant is 67 nm. g = 600 nm. (e) lattice constant is 536 nm. g = 120 nm. Right column with (c), (d) and (f): DNG ($\varepsilon = \mu = -1$) /air PCs. (c) lattice constant is 536 nm. g = 600 nm. (d) lattice constant is 67 nm. g = 600 nm. (f) lattice constant is 536 nm. g = 120 nm. The thicknesses of the two media in a period are identical.

and low group velocity to increase nonlinear effects during self-collimation, we just need to increase the lattice constant. Of course, if we choose g = 120 nm, the Gaussian beam will contain a lot of evanescent wave components. In this case, the field patterns in both MNG/ENG PC and DNG/air PC are coupled localized fields, as shown in Figs. 4(e) and 4(f). All the other parameters in Figs. 4(e) and 4(f) are the same with those in Figs. 4(a) and 4(c), respectively. The field pattern in Fig. 4(f) is similar to Fig. 2 in Ref. [18]. In MNG/ENG PC both propagating and evanescent wave components are amplified while in DNG/air PC only the evanescent wave components are enhanced. This is why the strength of localization in Fig. 4(e) is stronger than that in Fig. 4(f).

In the above calculations, we only considered lossless singe-negative materials. In practice, the losses in negative permeability of MNG medium and negative permittivity of ENG medium are inevitable especially at visible frequency. The loss in the materials will not only reduce the strength of collimated fields, but also decrease the transmittance due to absorption. In Fig. 5(a), we add losses in the PC used in Fig. 4(a). The real parts of ε_1 and μ_2 need be changed a little bit in order to obtain zero reflectance at the entrance of the structure when losses are involved. We select $\mu_1 = -0.965 + 0.002i, \varepsilon_2 = -1.035 + 0.002i$ and calculate the profile of the square of electric fields. One can see both the self-collimated fields and transmittance are decreases by the loss. To reduce the deleterious influence of loss, a possible way is to introduce gain medium such as quantum dots into the structure [27–29]. In Fig. 5(b),

#126182 - $15.00 USD Received 30 Mar 2010; revised 10 Jun 2010; accepted 16 Jun 2010; published 21 Jun 2010

we suppose the positive permeability of ENG medium and positive permittivity of MNG medium are embedded with gain medium, e.g., $\varepsilon_1 = \mu_2 = 1 - 0.002i, \varepsilon_2 = \mu_1 = -1 + 0.002i$, and calculate the profile of the square of electric fields. In comparison with Fig. 5(a), one can see both self-collimated fields and transmittance are recovered to those in the inset of Fig. 4(a). In other words, the effect of loss is compensated by the gain medium.

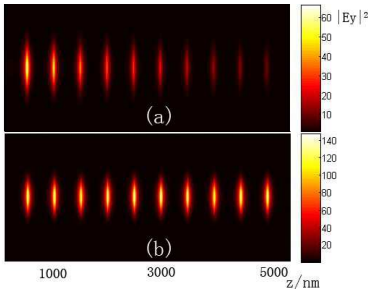

Fig. 5. The distributions of square of electrical fields in the PC used in Fig. 4(a) except that in (a) $\mu_1 = -0.965 + 0.002i, \varepsilon_2 = -1.035 + 0.002i$, and in (b) $\varepsilon_1 = \mu_2 = 1 - 0.002i$, $\varepsilon_2 = \mu_1 = -1 + 0.002i$, respectively.

5. Conclusion

In conclusion, self-collimation of a relatively broadband light beam is realized for a long distance in MNG/ENG PC because of the negative refraction across the two media that effectively cancel each other out. Both far and near fields can be collimated and boosted greatly in MNG/ENG PC. The enhancement of collimated fields will play an important role in the applications involving slow wave or nonlinear effect.

Acknowledgements

This research was supported by CNKBRSF (Grant No. 2006CB921701), by NSFC (Grant Nos. 10634050 and 10704055), by the Program for Key Basic Research of the Shanghai Science and Technology Committee (Grant No. 08dj1400301), by the Scientific Research Foundation for the Returned Overseas Chinese Scholars, State Education Ministry, and by the Ph.D. Programs Foundation of SEM (Grant Nos. 200802471091 and 20090072110052).

#126182 - $15.00 USD Received 30 Mar 2010; revised 10 Jun 2010; accepted 16 Jun 2010; published 21 Jun 2010